



Brief report

Independent and grouped 3D cell rotation in a microfluidic device for bioimaging applications

Srinivasu Valagerahally Puttaswamy^{a,*}, Nikhil Bhalla^{a,b,**}, Colin Kelsey^a, Gennady Lubarsky^a, Chengkuo Lee^c, James McLaughlin^{a,b,***}

^a Nanotechnology and Integrated Bioengineering Centre (NIBEC), School of Engineering, Ulster University, Jordanstown Shore Road, BT37 0QB, Northern Ireland, United Kingdom

^b Healthcare Technology Hub, Ulster University, Jordanstown Shore Road, BT37 0QB, Northern Ireland, United Kingdom

^c Department of Electrical & Computer Engineering, National University of Singapore, 4 Engineering Drive 3, 117576, Singapore



ARTICLE INFO

Keywords:

Cell-trapping

3D-rotation

Dielectrophoresis

Cell-imaging

ABSTRACT

Cell rotation reveals important information which facilitates identification and characterization of different cells. Markedly, achieving three dimensional (3D) rolling rotation of single cells within a larger group of cells is rare among existing cell rotation techniques. In this work we present a simple biochip which can be used to trap and rotate a single cell, or to rotate multiple cells relative to each other within a group of individual red blood cells (RBCs), which is crucial for imaging cells in 3D. To achieve single RBC trapping, we employ two parallel sidewall 3D electrodes to produce a dielectrophoretic force which traps cells inside the capturing chambers of the microfluidic device, where the hydrodynamic force then induces precise rotation of the cell inside the chamber. We have also demonstrated the possibility of using the developed biochip to preconcentrate and rotate RBC clusters in 3D. As our proposed cell trapping and rotation device reduces the intricacy of cell rotation, the developed technique may have important implications for high resolution 3D cell imaging in the investigation of complex cell dynamics and interactions in moving media.

1. Introduction

Microfluidic technology for manipulating individual cells, and small groups of cells has attracted a lot of attention in the field of biomedical engineering. Microfluidics allows precise positioning of eukaryotic and prokaryotic cells which facilitates their imaging under flow conditions in three-dimensional (3D) formats (Torino et al., 2016). Isolating and analysing single cells is crucial for understanding cell differentiation, cell transfection, and cell-cell interactions (Sackmann et al., 2014). Moreover, it is imperative to trap and analyse single cells to allow precise interpretation of therapeutic results to diagnose and understand diseases, which is conventionally done by considering large groups of cells (Luo et al., 2019). Single cell manipulation and analysis play a vital role in applications such as cell sorting (Jo et al., 2016), cell isolation (Gascoyne and Shim, 2014), droplet microfluidics (Guo et al., 2012) and

biosensing (Navin et al., 2011). In addition, on-chip single-cell culture, cell wall removal and reagent delivery have been demonstrated by special liquid flow fields contained on a single chip (Peng and Li, 2004). The rotational behaviour of cells is influenced by their morphology and is a potential diagnostic characteristic for malaria (Mohanty et al., 2004) and cancer (Zhao et al., 2018). Several techniques have been proposed previously for single cell rotation based on the optical, magnetic, and electrical properties of the cell (Elbez et al., 2011). In traditional microfluidic devices used for cell sorting or manipulation, it is only possible to observe a single two-dimensional (2D) view of a given cell. One possible solution to obtain more complete information about the cell is to rotate and image the cell from different angles. Previously, various methods have been proposed to manipulate single cells using electrical (Benhal et al., 2014; Chau et al., 2013; Han et al., 2013), acoustic (Ahmed et al., 2016; Collins et al., 2015), optical (Chiou et al.,

* Corresponding author.

** Corresponding author. Nanotechnology and Integrated Bioengineering Centre (NIBEC), School of Engineering, Ulster University, Jordanstown Shore Road, BT37 0QB, Northern Ireland, UK.

*** Corresponding author. Nanotechnology and Integrated Bioengineering Centre (NIBEC), School of Engineering, Ulster University, Jordanstown Shore Road, BT37 0QB, Northern Ireland, UK.

E-mail addresses: srini@ulster.ac.uk (S.V. Puttaswamy), n.bhalla@ulster.ac.uk (N. Bhalla), jad.mclaughlin@ulster.ac.uk (J. McLaughlin).

<https://doi.org/10.1016/j.bios.2020.112661>

Received 30 July 2020; Received in revised form 16 September 2020; Accepted 26 September 2020

Available online 28 September 2020

0956-5663/© 2020 Elsevier B.V. All rights reserved.

2005; Kolb et al., 2015), magnetic (Hejazian and Nguyen, 2016; Liu et al., 2009) and hydrodynamic (Hagiwara et al., 2012; Shelby and Chiu, 2004) forces. Among these methods, electrical methods are most extensively used due to their ease of use and to the low cost of device fabrication. In particular, dielectrophoresis (DEP) is the most prevalent method used for cell manipulation applications such as cell patterning (Puttaswamy et al., 2010), cell sorting (Valero et al., 2010) and cell switching (Puttaswamy et al., 2015).

DEP is the movement of a polarizable particle towards regions of either high or low electric field density when subjected to a non-uniform electric field (Adekanmbi and Srivastava, 2016; Cen et al., 2004). It occurs because of an imbalance of Coulombic forces between one side of a particle and the other. These Coulombic forces occur because the medium surrounding the particle becomes polarized with respect to the particle itself. In our experiments we are concerned with AC DEP, also sometimes known as classical DEP. Although this phenomenon occurs within kHz to GHz frequency range, higher frequencies (>100 kHz) have advantages in avoiding any static charging of the cells as well as reducing electrochemical reactions, and the gas bubble formation which may result from such reactions. We can distinguish negative dielectrophoresis (nDEP) from positive dielectrophoresis (pDEP) by the direction of particle movement with respect to the region of high field density. If the particle polarizes less in response to the applied field than the surrounding medium, then the particle will move away from regions of high field density (nDEP), while in the reverse situation the particle will move towards regions of high field density (pDEP). Polarizability of the cell and the surrounding medium depends on the frequency of the applied field. In general, for cells there will be a transition between nDEP and pDEP as the frequency of the applied field is increased at a point known as the crossover frequency. The polarizability of a cell will depend on its capacitance and its conductance, which in turn will depend on various features of the cell. Such features include (Pethig, 2017) the size and shape of the cell, the surface topography of the cell, the conductivities of the cytoplasm and nucleus, and the ratios of their volumes.

Rotation of particles in the presence of applied electric fields has been a known phenomenon since the late 1800s (Lamprecht and Michel, 1989), while early observations of the rotation of living cells due to applied electric fields were reported by Teixeira and Pimento (Teixeira-Pinto et al., 1960) in 1960. Previous work on cell rotation used rotating electric fields, produced by a quadruple electrode setup, to induce rotation in a single isolated cell (Benhal et al., 2014). This and similar electrode systems consist of combinations of 3D vertical/side-wall and bottom electrodes, the creation of which involves time consuming and complex processes such as metal deposition followed by mask lithography. More generally however, the cellular spin resonance (CSR) mechanism, which was reported for the first time by Pohl et al. (Pohl and Crane, 1971) can be achieved in a system as simple as a two pole electrode if cells are made to rotate independently within a larger group (Soffe et al., 2015). Pohl and Crane observed that cell rotation speed showed a sharply peaked distribution in response to the frequency of applied electric fields which led to the term CSR to describe the effect.

There are several different types of CSR (Pohl, 1983) which can be categorised according to number of cells rotating in the system and whether the field applied is of high frequency AC (greater than cell rotation speed) or DC/low frequency AC (less than cell rotation speed). In the DC/low frequency case the rotation is due to current depositing charge on the cell surface to form a dipole, followed by small random cell motions upsetting the alignment between this dipole and the applied field, leading to rotation. At higher frequencies there is insufficient time for the charge to build up via current deposition and charge imbalances are created by polarisation of the cell and surrounding medium. In all cases, CSR occurs because a torque is exerted on the cell, which forms a dipole, by the local electric field. In cases where the cell is rotating at a steady speed, this torque is balanced by an opposing torque due to drag on the cell. This drag may be any combination of viscous drag with the

surrounding medium, cell-surface friction, and drag induced by neighbouring cells, depending on the specific features of the experimental configuration.

For single cells the local external field is entirely due to the electrodes, hence for a rotational field to be induced, three or more electrodes are necessary and waveforms usually take the form of square voltage pulses applied to the various electrodes in sequence, or sinusoidal voltages applied across pairs of electrodes with a phase difference between orthogonal pairs. In the case where multiple cells are present, a cell may experience a rotating electric field from a combination of the field from the electrodes and the field produced by dipoles induced in neighbouring cells, meaning that the cell rotation can occur with two electrodes that have a time varying, usually sinusoidal, voltage applied between them. The speed of rotation will depend on the magnitude of the torque on the cell, which in turn will depend on the strength of the field as well as the strength of the electrical dipole of the cell and the difference in angle between the dipole and the field. The dependence on the field strength means that the speed of cell rotation will be influenced by the magnitude of the voltage applied as well as the conductivity of the liquid medium. In the scenario of multiple cells, it will also depend on the distance and relative orientation of the cells. In this case, the rotation direction will depend on the angle between the external field and the line joining the centres of the two cells (Mahaworasilpa et al., 1996). The dependence on the magnitude of the dipole and its lag with respect to the rotating field leads to a dependence on the dielectric properties of the cell itself. Using this fact in combination with models of cell structure, it is possible to measure the electro-rotational spectra of individual cells and extract information about the dielectric properties of the cell components. Since these properties e.g. such as membrane capacitance (Sukhorukov et al., 1993), cytoplasm conductivity (Huang et al., 1999), will vary with cell type as well as cell metabolism (Huang et al., 1996), this can be a useful tool for differentiating between cell type, as well as cell age and even for discriminating cancerous from non-cancerous cells (Lannin et al., 2016).

In this paper we present a novel microfluidic device for cell trapping and rotation. The applications of the device and techniques which we demonstrate are mainly associated with cell manipulation for full 3D surface imaging. The device can operate in two different modes. In the first mode of operation, which uses a 10 Vpp applied voltage at 1 MHz, pDEP is used to move single cells from the main channel and trap them in the trapping chamber, after which the applied voltage is turned off and the trapped single cells are rotated by hydrodynamic forces alone. In the second mode of operation, using a 10 Vpp applied voltage at 10 MHz, clusters of cells are trapped and rotated with this applied field remaining switched on throughout. There are two aspects to this rotation. The first is the rotation of the whole cluster combined, and the second is the rotation of individual cells within the cluster, which we refer to from here on as "rolling rotation". In this mode of operation we believe that the cell cluster rotation can be explained by the action of an unbalanced DEP force on the irregularly shaped cluster as a whole, while the rolling rotation is due to individual cells experiencing a rotating electric field due to a combination of the externally applied field, along with the contribution of the dipoles of nearby cells. This is similar to the CSR mechanism discussed above described by Pohl (1983). We used red blood cells to demonstrate the feasibility and application of the device for cell trapping and rotation. This concept can be translated to all cells of similar dimensions, suggesting that this work may represent an important innovation in lab on chip systems.

2. Fabrication, chip design and working principle

The complete details of the fabrication of the PDMS microchannel were reported in our previous publication (Puttaswamy et al., 2015). In summary, the conventional soft lithography process was used to fabricate polydimethylsiloxane (PDMS) microfluidic channels. Briefly, the silicon substrate was cleaned using the piranha method, before

patterning SU-8 negative photoresist (SU-8 25, MicroChem Corp, USA) by photolithography. A PDMS pre-polymer and cross linker were mixed thoroughly with a weight ratio of 10:1 and subjected to degassing before and after pouring on the silicon master mould. Further, the master mould was placed in an electric oven and cured at 90 °C for 1 h. The cured PDMS was peeled off, punched with inlets/outlets and bonded onto a glass substrate after treating with oxygen plasma (Harrick Plasma Inc, USA) for 60 s. The device was then placed on a hotplate at 100 °C for 30 s to enhance bonding between the PDMS and glass substrate, creating a closed micro fluidic chamber.

After fabricating PDMS channels, to embed 3D electrodes within the electrode microchannels, the microfluidic device on the glass substrate was placed on the hot plate at 80 °C and heated for 5 min. The electrode material, indium alloy (Indalloy® 19 In–Bi–Sn Fusible Alloy), which is essentially stable and inert wire, was inserted into the inlet of the electrode channel as shown in Fig. 1(a) (i). When pushed down against the heated glass, it melts and flows along the electrode microchannel as represented in Fig. 1(a) (ii). The flow of electrode material continues towards the outlet of the electrode channel as illustrated in Fig. 1(a) (iii). The procedure is repeated to fabricate a parallel electrode in the opposite channel. Conducting wire electrodes were inserted into both inlets and outlets for electrical connection to the external circuit which applies a signal of the required voltage and frequency during DEP manipulation. The device was removed from the hot plate, and allowed to cool to room temperature, which allows the electrode material to solidify in the electrode channel to form the solid 3D sidewall electrodes.

The microfluidic device designed for single cell and cell cluster rotation consists of three main components as shown in Fig. 1(b). The first one is the main channel with 15 µm width and 70 µm height for cell sample and buffer flow. The optimum width of 15 µm minimises the gap between the two parallel side wall electrodes, which maximises the DEP

force applied to the cells. The second component is the electrode channels with 50 µm width and 70 µm height, which permit the free flow of electrode material, to fill the channels before solidifying to form the sidewall 3D electrodes. The third component is the PDMS structure between the main channel and electrode channel which forms cell trapping chambers to accommodate single RBCs during DEP trapping. The cell trapping chambers are each designed to accommodate only a single cell at a time, once the cell is pulled towards it due to pDEP force. The trapping chambers each have dimensions of 12 µm width, 14 µm depth and 70 µm height. A microscopic bright field image of the actual device is shown in Fig. 1(c).

RBCs used in this study were obtained from finger prick samples taken from the pad of the middle finger of donors from whom informed consent had been obtained. Samples were taken using BD Genie Lancets following the manufacturer recommended procedure. The samples were then transferred into anticoagulant-coated (ethylenediamine tetraacetic acid, EDTA) micro-centrifuge tubes and the RBCs separated from the other blood components by centrifugation. The RBCs were re-suspended in Phosphate Buffered Saline (PBS). Gentle sonication was used on the RBC/PBS suspension to ensure that the RBCs were uniformly dispersed. At the same time the microfluidic channel was washed using a solution of 1% surfactant, Pluronic F-127 (Sigma-Aldrich, Singapore) in PBS solution for 30 min to prevent adhesion of cells in the main channel. The RBC/PBS solution was pumped into the channel at a low flow rate using a syringe pump (New Era Pump Systems, USA). This was followed by the application of the electric field. The signal applied to the electrodes to generate the electric field was produced by amplifying an AC signal from a signal generator (Tektronix) with a power amplifier (Ophir RF, USA). The voltage of the amplified signal ranged from 5 to 20 Vpp with frequency in the range from 1 kHz to 60 MHz with parameters verified by monitoring the amplified signal using an oscilloscope.

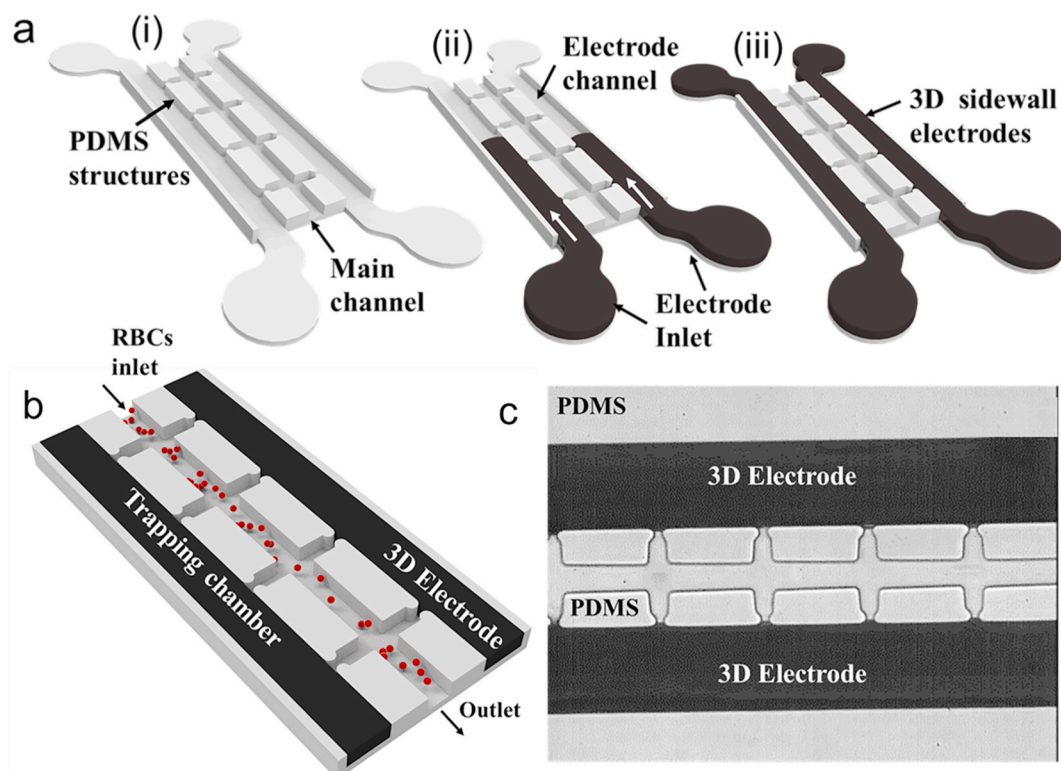


Fig. 1. Fabrication and working principle of microfluidic device. (a) illustration of the fabrication of the side wall 3D electrodes (i) introduction of electrode material via inlet of electrode channel (ii) maintaining the flow of electrode material through the channel (iii) filling the electrode channel completely and exiting via channel outlet (b) pictorial representation of device design, working principle, showing cell trapping region, electrode channel for introducing electrode material and main channel to introduce cell sample (c) bright field image of the actual microfluidic device representing all three regions with trapping chamber formed between two PDMS structures.

3. Results and discussion

3.1. Single cell trapping

The device contains 3D electrodes with a height of 70 μm , providing enough space for a single cell or group of cells to freely rotate without cell clogging. These electrodes produce a field that is highly uniform in the z direction but non-uniform in the x-y plane such that there is a strong convergence of the electric field lines in the x-y direction near the trapping region when an AC voltage is applied to the electrodes. This can produce a strong pDEP force for cell trapping.

During trapping, cells were introduced slowly at a flow rate of 0.01 $\mu\text{l}/\text{min}$ with a distribution of 5–6 cells per 10 μm length. Once the flow stabilized, cells were uniformly distributed across the main channel and an AC electric field of 10 Vpp at 1 MHz was applied via the 3D electrodes. The curvature of the field lines around the electrodes resulting from the applied voltage creates an electric field maxima in the trapping chamber, close to the electrode surface.

The resulting pDEP force attract RBCs towards the region of maximum electric field, which in turn causes the RBCs to become trapped in the trapping chamber as pictorially illustrated in Fig. 2(a). The size of the trapping chamber was designed to accommodate a single RBC, preventing entry of additional cells into the trapping chamber, and the bright field image of actual RBC trapped in the trapping chamber of the microfluidic device is shown in Fig. 2(b). The 3D side wall electrodes facilitate easy trapping of RBCs irrespective of their position in the main microfluidic channel, because of the consistent non-uniform electric field along the full height of the channel. To simulate electric field distribution in the trapping region, we used the AC/DC module of COMSOL Multiphysics. The geometry and dimensions of the electrodes in the finite element model were selected to match the real fabricated device. The model included the main fluid channel, the PDMS insulating region, and the electrodes as well as a small section of the insulating regions above and below the device. The electrical insulation boundary condition was applied to all external boundaries of the model except for the external faces of the two electrodes, one of which was grounded on all of its external boundary faces while the other had the electric potential applied to its external boundary faces. Fig. 2(c) shows lines of electric potential and is shaded according to electric field strength. The area near the trapping region is shown with an applied voltage of 10 Vpp at 1 MHz. The field strength is maximum in the trapping chamber close to the electrode surface, which causes the single cell to be attracted into the trapping chamber due to pDEP. The red arrows illustrate the direction of the divergence of the electric field, which determines the direction of the dielectrophoretic force that would be experienced by a cell or particle at that point. The model was solved in the frequency domain in three dimensions, with the included figure showing the results at a slice through

the model centre. The electric field was similar across the entire height of the channel.

3.2. Single cell rotation

The experimental evaluation of hydrodynamic cell rotation was done by using trapped RBCs in the trapping chambers. RBCs are small and biconcave in shape making them perfect for studying rotational influences (Diez-Silva et al., 2010). Once a single RBC had been trapped by applying an electric potential of 10 Vpp at 1 MHz, this electric field was then turned off and the flow rate of the buffer was increased to 2 $\mu\text{l}/\text{min}$ to expel un-trapped cells in the main channel, while allowing the trapped cell to freely rotate in the trapping chamber subject to hydrodynamic microvortex forces. The speed of rotation could be controlled by altering the flow rate of the buffer in the main channel. Due to the fluid flow in the channel, opposite sides of the cell are subjected to different fluid flow velocities, inducing a torque on the cell which results in cell rotation.

We used flow rates of 2 $\mu\text{l}/\text{min}$ and the position and orientation of an RBC at time intervals of 1,3,5,7, 9 and 11 s is represented in Fig. 3(a–f). The trapping and rolling rotation of a single RBC is represented pictorially in Fig. 3(g) while actual rotation of the RBC is visualized in supplementary result S1. The RBC shows a minor translational motion in the horizontal and vertical directions (X and Y), while rotating in the trapping chamber, so that the cell can be imaged from many orientations covering the entire cell surface. The mean X and Y position throughout the entire video segment was calculated, and the displacement from this position at each point in time is plotted in Fig. 3(h). Since the cells are not perfectly circular, it was also possible to fit an ellipse to each cell mask and plot the angle of the major axis of the ellipse over time as seen in Fig. 3(i). The gradient of this plotted line was then used to determine the speed of the cell's rotation. This method of cell rotation is simple, biosafe, and cost effective, and there is no need for coating or pre-treatment of the cell to allow rotation to be induced.

3.3. Multi cell trapping and rotation

In our current work we demonstrate how individual cells and groups of cells can be rotated to observe 3D features with a high throughput i.e. simultaneously rotating group of cells within the microfluidic device. This has important implications in advanced bioimaging where differences within a given population of cells can be identified in a short period of time (due to grouped rotation of cells). In addition, in our previous work (Puttaswamy et al., 2015, 2019), we used silver conductive adhesive and carbon nano-powder as the electrode material composite which was injected into the electrode channel to fabricate the 3D electrodes. In contrast, this work employs indium alloy as the

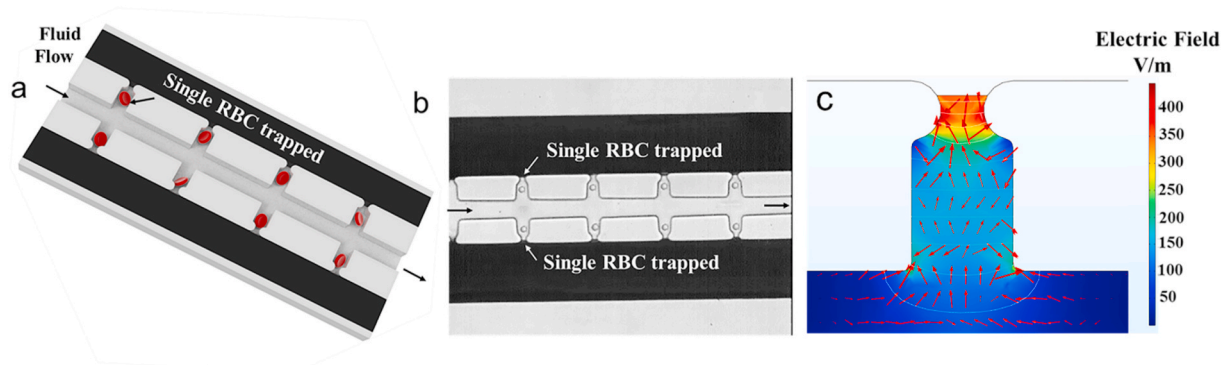


Fig. 2. Single cell trapping due to pDEP force. (a) pictorial representation of cell trapping with the application of electric field (b) microscopic bright field image, showing trapping of a single RBC in each microwell, after washing untrapped cells in the main channel while keeping electric field on (c) Simulation of electric field distribution with arrows representing the divergence of the field and indicating pDEP force direction, produced using COMSOL Multiphysics.

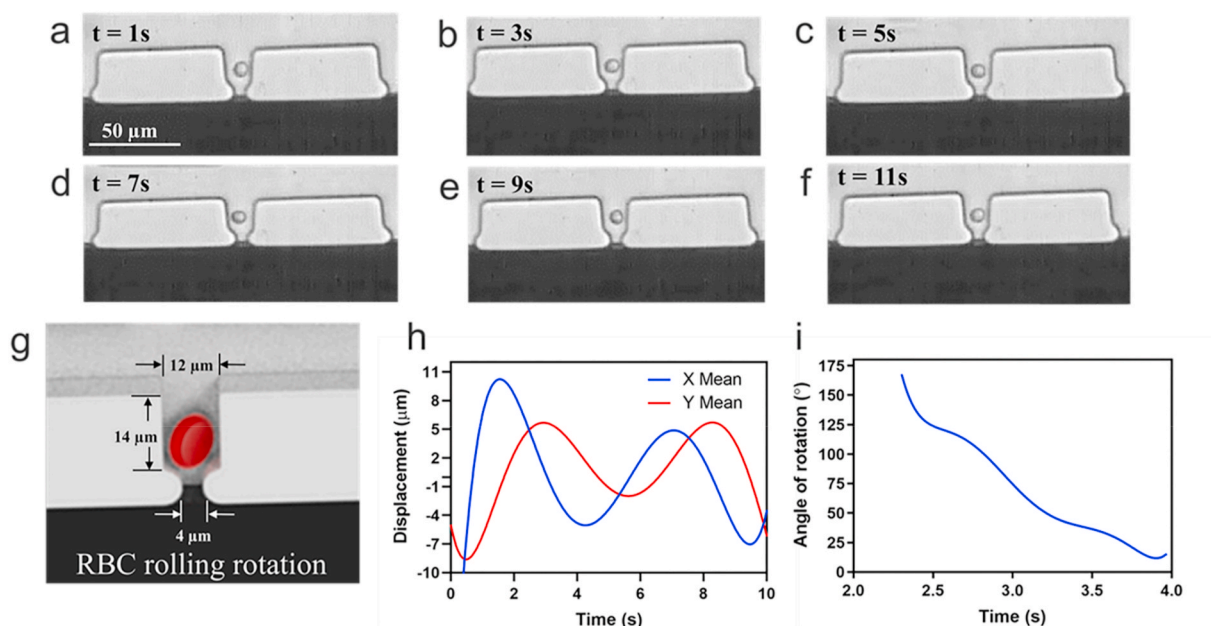


Fig. 3. Single cell rotation within the microwell. The single RBC was attracted from the main channel towards the trapping region by pDEP force. The trapped cells are then rotated within the microwell by hydrodynamic microvortex forces due to the flow in the main channel. The cell rotates and changes its position within the microwell (a–f) shown at different time intervals of $t = 1$ s, 3 s, 5 s, 7 s, 9 s and 11 s respectively. (g) Illustration clarifying shape and position of single RBC while rotating in the trapping chamber with critical dimensions indicated (h) X and Y translational movement about mean trapped position of single RBC within the microwell caused by hydrodynamic vortex flow (i) time plot of angular rotation of single RBC in the microwell caused by hydrodynamic microvortex flow.

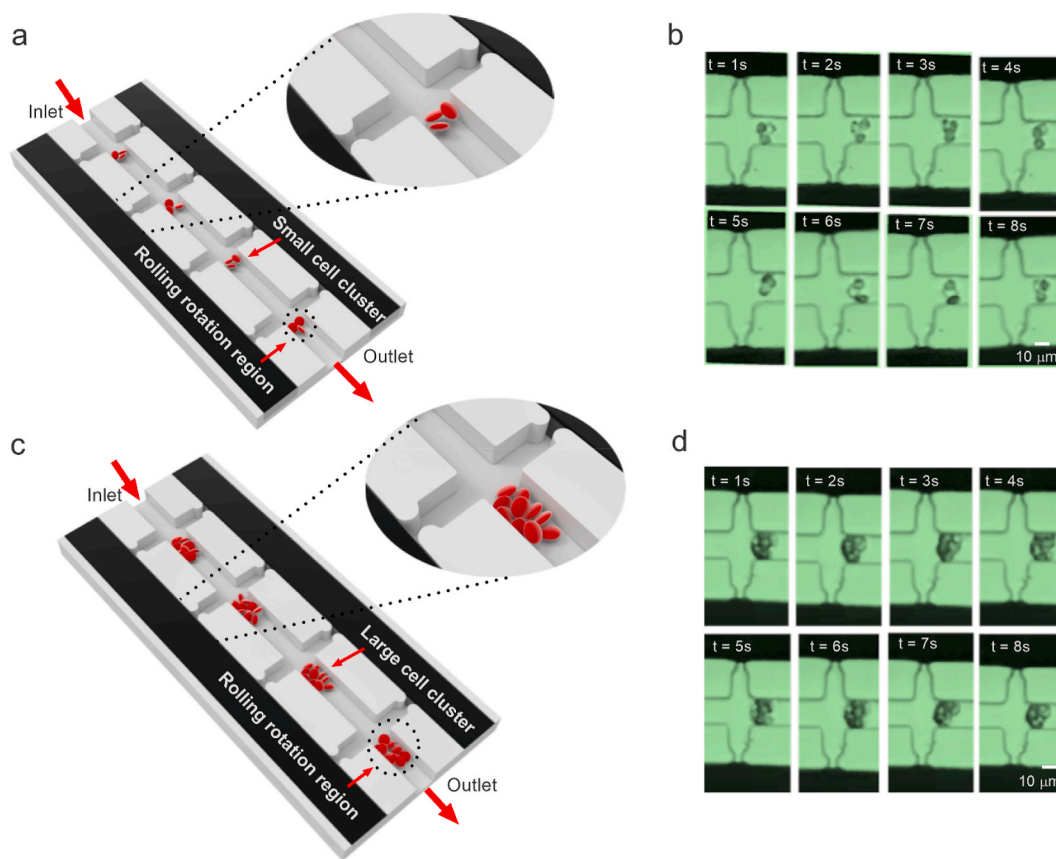


Fig. 4. Multi cell rotation at different cell concentrations (a, b) diagram and microscopic image of group of 3 cells, interacting to rotate relative to each other with the application of 10 Vpp at 10 MHz as long as the electric field is on (c, d) diagram and microscopic image group of around 10 cells rotating, tumbling and rolling over each other with the application 10 Vpp at 10 MHz, and with increased cell concentration.

electrode material, which is used to fabricate the sidewall 3D electrodes (Ma et al., 2016). One advantage of indium over the silver nanopowder composite used in our previous work is that use of indium alloy simplifies fabrication of the electrodes. There is no need to have precise control over the flow rate during injection of the electrode material into the electrode channel. A second advantage is that the electrical resistivity of indium alloy, at 0.52×10^{-6} ohm-m, is very low compared to the silver nanopowder composite in our previous work. This results in a higher field strength for a given applied voltage and frequency and has enabled a new application—the rolling rotation of cells within microfluidic chips.

Our design features a large electrode inlet which we completely fill before driving electrode material through the electrode channel. After we fill the large electrode inlet, the plunger attached to the micromanipulator is used to push material from the filled inlet through the electrode channel. This technique facilitates free flow of electrode material, without requiring vacuum (Chatzimichail et al., 2018) while still completely occupying the electrode channel without creating any air-gaps. The simplified channel design allows the electrode material to properly reach all sections of the electrode channel whereas a more complex, branched or narrow design, or one with additional curvature would have introduced excessive resistance to the flow of the electrode material. Further it provides a consistent electric field distribution along the height of the channel, necessary for efficient cell micromanipulation, and for generating rolling rotational motion.

To show its versatility, we use the device to demonstrate both small and large RBC cluster rotation. The overall cluster rotation is due to the unbalanced DEP forces on the irregularly shaped cluster overall, while the rolling rotation of individual cells within the cluster is due to the interaction of the dipoles in the cells (Ahmed et al., 2016) with the external field as well as the fields generated by the dipoles of neighbouring cells. The direction and the speed of rolling rotation depends on the position of the cells relative to each other and to the external field. The experimental demonstration of multi cell rotation is represented in Fig. 4.

During small RBC cluster trapping and rotation, cells were introduced slowly at a flow rate of $0.01 \mu\text{l}/\text{min}$ with a distribution of 3–5 cells per $10 \mu\text{m}$ length. To prevent clogging of RBCs and to promote free flow of individual cells we have used PDMS structures as flow filters with a narrow gap between them at the inlet. With this arrangement, we could control the number of cells flowing in the main channel. The number of RBCs present in the main channel was comparatively low when trapping single cells, whereas the number of RBCs was comparatively high for trapping large cell clusters. When an AC electric field of $10 V_{pp}$ at 10 MHz is applied via 3D electrodes three to four cells move towards each other, to form a small RBC cluster in the trapping region as represented in Fig. 4(a and b) and in supplementary result S2. The cells begin rolling rotation on a 3D axis, interacting with each other, while rolling continuously whilst the electric field is on. To trap and rolling rotate large clusters, cells were introduced slowly at a flow rate of $0.01 \mu\text{l}/\text{min}$ with a distribution of 10–12 cells per $10 \mu\text{m}$ length. When an AC electric field of $10 V_{pp}$ at 10 MHz is applied via 3D sidewall electrodes, around ten cells move towards each other to form a large cluster in the trapping region, as represented in Fig. 4(c and d) and in supplementary result S3. When the electric field is on, the cells rotate as a group, tumble, and interact with each other, while simultaneously undergoing rolling rotation on their own axes. When multiple cells are present, they accumulate to form clusters and rotate due to unbalanced DEP forces. Individual cells in the cluster experience a rotating field that results from a combination of externally applied electric field, along with the contribution of the dipoles of adjacent cells, resulting in rolling rotation. The chief advantage of this proposed method is that, the number of cells in the cluster could be controlled by varying the distribution of cells per micrometre length in the main channel. In addition, every RBC in the cell cluster, subjected to rolling rotation, which is crucial in 3D cell imaging and to study cell to cell interactions.

3.4. Influence of applied voltage and frequency on cell rotation speed

The influence of applied frequency in the range of 10–60 MHz at a constant voltage of $10 V_{pp}$ on the rotation of an RBC cluster is represented in Fig. 5(a). The rotation of RBC clusters starts even at 5 MHz and increases linearly as the frequency is increased, attaining a maximum value of ~ 210 rpm at 60 MHz. The trend of linear increase in rotational speed with increase in frequency is as represented in Fig. 5(c). The rolling rotation of RBCs could be properly visualized with a voltage of $10 V_{pp}$ and frequency of 10 MHz as evident from the supplementary result S3. The application of frequencies above 60 MHz is not advisable as it may have an undesirable effect on cell viability. The rotational response of RBC clusters for the applied voltage was investigated in the range of 1– $10 V_{pp}$ with constant applied frequency of 10 MHz and is represented in Fig. 5(b).

The variation of rotational speed is also linear across the voltage range investigated with the RBC cluster starting to slowly rotate from as low as $2 V_{pp}$ as indicated in Fig. 5(d). Initially at low voltage, the cluster rotates as a unit without any rolling action, however when the voltage starts to increase beyond $5 V_{pp}$, the RBCs start to rolling rotate over each other while this phenomenon could be clearly visualized at $10 V_{pp}$. This behaviour continues, with increased speed as we increase the voltage right up to $20 V_{pp}$ which was the maximum voltage investigated. The intercellular gap decreases as voltage magnitude increases above $10 V_{pp}$. At high applied voltage, $20 V_{pp}$, cells tumbling over each other along with rolling rotation results in increased intercellular friction. To overcome this problem, it is desirable to keep the applied voltage below $15 V_{pp}$.

4. Conclusions

In this work, two applications, a microfluidic approach to rolling rotate a single cell, and an electrokinetic approach to rotate a cell cluster, have been successfully presented. The design and fabrication of a microfluidic device has been outlined. The device consists of a trapping chamber which has been shown to efficiently trap single cells and enable smooth rolling rotation. The main microfluidic channel has also been shown to be able to act as a trapping site for cell clusters to rotate and for cells to flow along the main channel when the electric field is turned off. The experimental result of trapping single cells via pDEP force was well supported by simulation results. We employed a simple and cost-effective method to fabricate the 3D side wall electrodes, which readily integrated with the microfluidic device. The ease of electrode fabrication reduces electrode alignment issues and removes any requirement to use expensive metal deposition systems. The proposed device could be used for example to perform 3D imaging to analyse the internal dynamics of a cell, to study cell dielectric properties, or to study cell-to-cell interactions for a better understanding of mechanisms underlying many diseases. Alternatively it could function as part of a platform for disease diagnosis or for drug discovery.

Author contributions

SVP performed all experiments related to sample preparation, design and fabrication of microfluidic device. CK, GL assisted SVP in experiments related to cell rotation and sample preparation. JM planned and supervised the overall work. SVP prepared the initial manuscript draft with input from NB, JM, VL, CK and SVP, NB, JM, VL revised the final version of the manuscript and all authors approved the submission.

CRediT authorship contribution statement

Srinivasu Valagerahally Puttaswamy: Conceptualization, Methodology, Validation, Formal analysis, Investigation, Writing - original draft. **Nikhil Bhalla:** Writing - original draft. **Colin Kelsey:** Writing - original draft. **Gennady Lubarsky:** Software, Visualization. **Chengkuo**

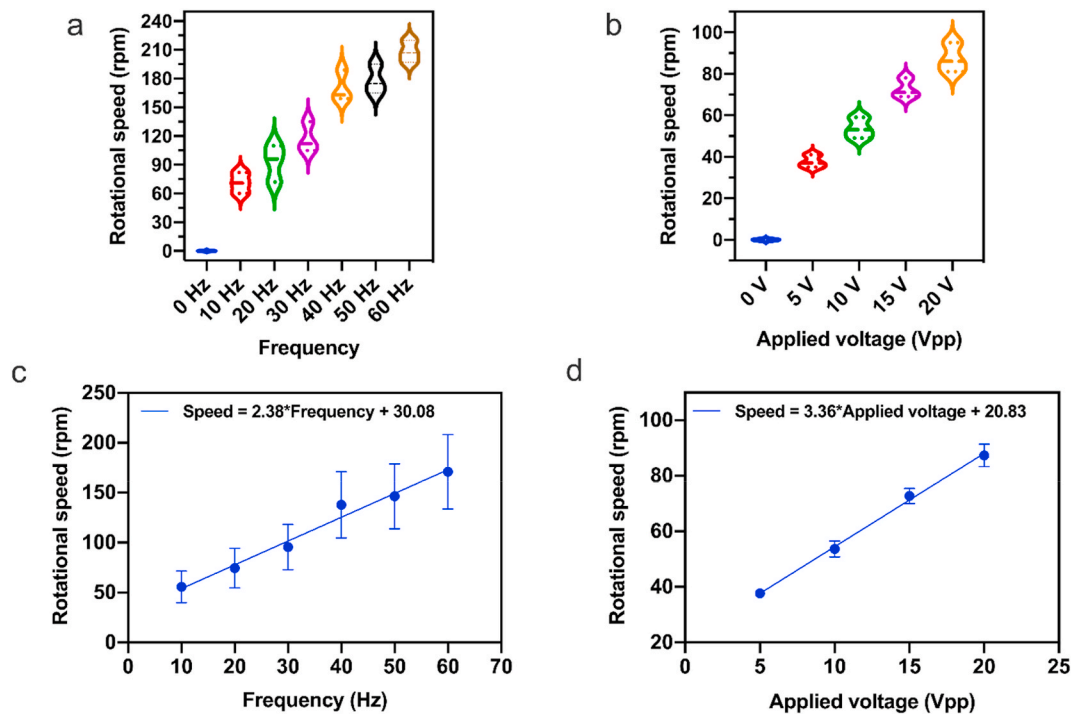


Fig. 5. Variation of rotational speed of RBC clusters with respect to the applied frequency and voltage (a) Rotational speed of the RBCs in PBS solution when applied frequency vary from 0 MHz to 60 MHz at 10 Vpp (b) Rotational speed of the RBC clusters in PBS solution when applied voltage vary from 0 Vpp to 20 Vpp at 10 MHz. (c) and (d) represent the proportional linear variation in rotational speed versus applied voltage and frequency.

Lee: Validation, Resources. **James McLaughlin:** Writing-reviewing and editing, Resources.

Declaration of competing interest

The authors declare that there are no known conflicts of interest associated with this publication.

Acknowledgements

This work was supported by funding under the Invest Northern Ireland - Connected Health Innovation Centre (CHIC) Competence Centre and the European Union's INTERREG VA Programme, managed by the Special EU Programmes Body (SEUPB) – the Eastern Corridor for Medical Engineering (ECME).

Appendix A. Supplementary data

Supplementary data to this article can be found online at <https://doi.org/10.1016/j.bios.2020.112661>.

References

- Adekanmbi, E.O., Srivastava, S.K., 2016. *Lab Chip* 16, 2148–2167.
 Ahmed, D., Ozcelik, A., Bojanala, N., Nama, N., Upadhyay, A., Chen, Y., Hanna-Rose, W., Huang, T.J., 2016. *Nat. Commun.* 7.
 Benhal, P., Chase, J.G., Gaynor, P., Oback, B., Wang, W., 2014. *Lab Chip* 14, 2717–2727.
 Cen, E.G., Dalton, C., Li, Y., Adamia, S., Pilarski, L.M., Kaler, K.V.I.S., 2004. *J. Microbiol. Methods* 58, 387–401.
 Chatzimichail, S., Supramaniam, P., Ces, O., Salehi-Reyhani, A., 2018. *Sci. Rep.* 8, 1–10.
 Chau, L.-H., Liang, W., Cheung, F.W.K., Liu, W.K., Li, W.J., Chen, S.-C., Lee, G.-B., 2013. *PLoS One*, vol. 8.
 Chiou, P.Y., Ohta, A.T., Wu, M.C., 2005. *Nature* 436, 370–372.
 Collins, D.J., Morahan, B., Garcia-Bustos, J., Doerig, C., Plebanski, M., Neild, A., 2015. *Nat. Commun.* 6, 8686.
 Diez-Silva, M., Dao, M., Han, J., Lim, C.-T., Suresh, S., 2010. *MRS Bull. Res. Soc.* 35, 382.
 Elbez, R., McNaughton, B.H., Patel, L., Pienta, K.J., Kopelman, R., 2011. *Stress Drug*

- Gascoyne, P.R.C., Shim, S., 2014. *Cancers* 6, 545–579.
 Guo, M.T., Rotem, A., Heyman, J.A., Weitz, D.A., 2012. *Lab Chip* 12, 2146–2155.
 Hagiwara, M., Kawahara, T., Arai, F., 2012. *Appl. Phys. Lett.* 101, 74102.
 Han, S.-I., Joo, Y.-D., Han, K.-H., 2013. *Analyst* 138, 1529–1537.
 Hejazian, M., Nguyen, N.-T., 2016. *Biomicrofluidics* 10, 44103.
 Huang, Y., Wang, X.-B., Becker, F.F., Gascoyne, P.R.C., 1996. *Biochim. Biophys. Acta Biomembr.* 1282, 76–84.
 Huang, Y., Wang, X.-B., Gascoyne, P.R.C., Becker, F.F., 1999. *Biochim. Biophys. Acta Biomembr.* 1417, 51–62.
 Jo, Y., Shen, F., Hahn, Y.K., Park, J.-H., Park, J.-K., 2016. *Micromachines* 7, 56.
 Kolb, T., Albert, S., Haug, M., Whyte, G., 2015. *J. Biophot.* 8, 239–246.
 Lamprecht, I., Mischel, M., 1989. Cellular spin resonance. In: *Electroporation and Electrofusion in Cell Biology*. Springer, pp. 23–35.
 Lannin, T., Su, W.-W., Gruber, C., Cardle, I., Huang, C., Thege, F., Kirby, B., 2016. *Biomicrofluidics* 10, 64109.
 Liu, W., Dechev, N., Foulds, I.G., Burke, R., Parameswaran, A., Park, E.J., 2009. *Lab Chip* 9, 2381–2390.
 Luo, T., Fan, L., Zhu, R., Sun, D., 2019. *Micromachines* 10, 1–31.
 Ma, Z., Teo, A.J.T., Tan, S.H., Ai, Y., Nguyen, N.-T., 2016. *Micromachines* 7, 216.
 Mahaworasilpa, T.L., Coster, H.G.L., George, E.P., 1996. *Biochim. Biophys. Acta Biomembr.* 1281, 5–14.
 Mohanty, S.K., Uppal, A., Gupta, P.K., 2004. *Biotechnol. Lett.* 26, 971–974.
 Navin, N., Kendall, J., Troge, J., Andrews, P., Rodgers, L., McIndoo, J., Cook, K., Stepansky, A., Levy, D., Esposito, D., 2011. *Nature* 472, 90.
 Peng, X.Y., Li, P.C.H., 2004. *Anal. Chem.* 76, 5273–5281.
 Pethig, R.R., 2017. *Dielectrophoresis: Theory, Methodology and Biological Applications*. John Wiley & Sons.
 Pohl, H.A., 1983. *Int. J. Quant. Chem.* 24, 161–174.
 Pohl, H.A., Crane, J.S., 1971. *Biophys. J.* 11, 711–727.
 Puttaswamy, S.V., Fishlock, S.J., Steele, D., Shi, Q., Lee, C., McLaughlin, J., 2019. *Biomed. Phys. Exp. Express* 5, 55003.
 Puttaswamy, S.V., Sivashankar, S., Chen, R.J., Chin, C.K., Chang, H.Y., Liu, C.H., 2010. *Biotechnol. J.* 5, 1005–1015.
 Puttaswamy, S.V., Xue, P., Kang, Y., Ai, Y., 2015. *Biomed. Microdevices* 17, 4.
 Sackmann, E.K., Fulton, A.L., Beebe, D.J., 2014. *Nature* 507, 181–189.
 Shelby, J.P., Chiu, D.T., 2004. *Lab Chip* 4, 168–170.
 Softe, R., Tang, S.-Y., Baratchi, S., Nahavandi, S., Nasabi, M., Cooper, J.M., Mitchell, A., Khoshmanesh, K., 2015. *Anal. Chem.* 87, 2389–2395.
 Sukhorukov, V.L., Arnold, W.M., Zimmermann, U., 1993. *J. Membr. Biol.* 132, 27–40.
 Teixeira-Pinto, A.A., Nejeleski Jr., L.L., Cutler, J.L., Heller, J.H., 1960. *Exp. Cell Res.* 20, 548–564.
 Torino, S., Iodice, M., Rendina, I., Coppola, G., Schonbrun, E., 2016. *Sensors* 16, 1326.
 Valero, A., Braschler, T., Demierre, N., Renaud, P., 2010. *Biomicrofluidics* 4, 22807.
 Zhao, Y., Jia, D., Sha, X., Zhang, G., Li, W.J., 2018. *Micromachines* 9, 118.